Magnetic resonance spectroscopy on the spin-frustrated magnets YBaCo$_3$MO$_7$ (M=Al, Fe)

M. Iakovleva,[1,2,3] S. Zimmermann,[1,2] J. Zeisner,[1,2] A. Alfonsov,[1] H.-J. Grafe,[1] M. Valldor,[4]
E. Vavilova,[3] B. Büchner,[1,2] and V. Kataev[1]

[1]*Leibniz Institute for Solid State and Materials Research IFW Dresden, 01069 Dresden, Germany*
[2]*Institute for Solid State Physics, TU Dresden, 01069 Dresden, Germany*
[3]*Zavoisky Physical-Technical Institute of the Russian Academy of Sciences, 420029 Kazan, Russia*
[4]*Max-Planck-Institute for Chemical Physics of Solids, 01187 Dresden, Germany*

We present experimental results of combined electron spin resonance (ESR) and nuclear magnetic resonance (NMR) measurements on single crystals of the Swedenborgite-type compounds YBaCo$_3$MO$_7$ (M=Al, Fe). The magnetic lattice of these materials can be described as stacks of strongly geometrically frustrated kagome layers built up of Co^{2+} ($S = 3/2$) ions. Due to the Co-M site intermixing, there are M-type defects in the kagome planes as well as magnetic Co ions at the interplanar positions. Previous investigations revealed large antiferromagnetic (AFM) Curie-Weiss temperatures in both compounds. Yet no AFM long-range order but a spin glass behavior at low temperatures has been observed. Using ^{27}Al NMR as well as Co^{2+} and Fe^{3+} ESR spin probes that are sensitive to local magnetic properties at different crystallographic sites, we have identified two magnetic subsystems in both compounds and have studied their distinct properties. In particular in the case of YBaCo$_3$AlO$_7$, we have observed a gradual development of the spin correlations in the two-dimensional (2D) kagome planes containing nonmagnetic Al defects and the establishment of a 3D frozen glasslike spin state of the interplanar Co ions at lower temperatures. We have found that despite a strong dependence of the ordering temperature in the kagome layers on the type of the M ion (magnetic or nonmagnetic), the final 3D static ground state sets in at rather similar temperatures. We argue that the peculiar spin dynamics and a disordered magnetic ground state of the studied compounds result from the interplay of strong magnetic frustration and intrinsic structural disorder arising due to the intersite mixing of Co and M atoms.

I. INTRODUCTION

Cobalt oxides currently attract much attention because they show a rich variety of interesting physical properties such as charge stripes in La$_{2-x}$Sr$_x$CoO$_4$ [1], a spin-orbital superstructure in strained ferrimagnetic perovskite cobalt oxides [2], unconventional superconductivity [3,4], large thermoelectric power [5], a spin state transition in SrCo$_{0.5}$Ru$_{0.5}$O$_{3-\delta}$ [6], etc. Another interesting feature of some cobaltates is the presence of a high degree of magnetic frustration due to competing exchange interactions.

One reason of magnetic frustration is a specific topology of the spin lattice where antiferromagnetic alignment of spins cannot be achieved simultaneously for all bonds connecting the spins. Frustration due to geometry may yield various exotic ground states ranging from resonating valence bond spin liquids to spin ice [7] and spin-chirality [8]. Most of such systems can be described by a simple Heisenberg Hamiltonian with nearest-neighbor antiferromagnetic interactions on a corner-sharing lattice. A classical example of the latter is a kagome lattice in two dimensions, which is a fundamental but experimentally elusive frustrated magnet [9,10]. Among the compounds with kagome lattices of antiferromagnetically coupled spins, the transition-metal-based Swedenborgites are probably the only ones where the crystallographic space group is noncentrosymmetric and polar ($P6_3mc$). These facts allow for a manifold of magnetic ground states to form and for the emergence of magnetoelectric coupling, e.g., via Dzyaloshinsky-Moriya interaction [11,12]. While for some compositions like YBaCo$_4$O$_7$ [13], CaBaCo$_4$O$_7$ [14], and CaBaCo$_2$Fe$_2$O$_7$ [15] long-range spin order is

reported, others like YBaCo$_{4-x}$Zn$_x$O$_7$ ($x = 0 - 3$) [16] and Y$_{0.5}$Ca$_{0.5}$BaCo$_4$O$_7$ [17] exhibit spin-glass or spin-liquid properties, respectively.

Introducing magnetic or nonmagnetic impurities to the frustrated compound strongly affects the ground state of the system and leads to the appearance of a rich variety of spin states, such as spin liquids, spin glasses, and clusters or long-range magnetic order. From the previous studies of the title compounds, it is known that both materials have magnetic ions with strong antiferromagnetic coupling but do not show any long-range order even at low temperatures [18,19]. In YBaCo$_3$FeO$_7$, the freezing of spin correlations was observed at temperatures $T_f \approx 50$ K, whereas for the YBaCo$_3$AlO$_7$, the magnetization measurements show a highly degenerate spin state with a freezing temperature $T_f = 16.8$ K. It was reported that the ground state of YBaCo$_3$AlO$_7$ is a spin glass with randomly frozen domains [19].

In this paper, we present an investigation of the effects of structural disorder due to the Co/M intermixing and the influence of magnetic and nonmagnetic defects on the magnetic properties of the Swedenborgite compounds YBaCo$_3$MO$_7$ (M=Al, Fe) by nuclear magnetic resonance (NMR) and electron spin resonance (ESR) spectroscopies complemented by magnetization measurements. Measurements of high-field ESR (HF-ESR) of Fe^{3+} ions at the interplane sites of YBaCo$_3$FeO$_7$ have revealed short-range quasistatic spin correlations setting in at $T_{f2} \approx 60$ K, which is much smaller than the in-plane transition temperature $T_{f1} = 590$ K [18]. No signatures of the long-range order have been found below T_{f2}. A strongly inhomogeneous distribution of local fields in YBaCo$_3$AlO$_7$, quasistatic on the ESR time scale already
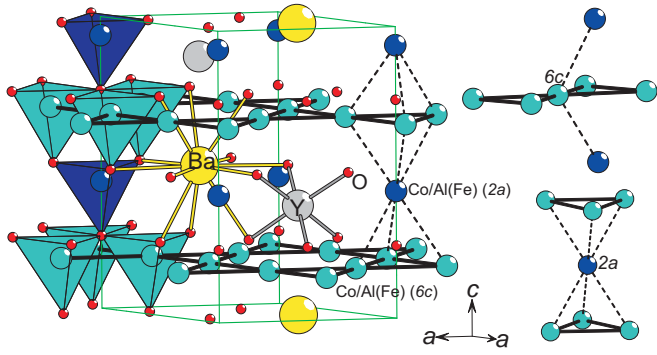
FIG. 1. A perspective view of the atomic structure of $YBaCo_3MO_7$ ($M =$ Al, Fe). The bonding lines between the metals and oxygen atoms show the oxygen interrelation of Y and Ba. The kagome plane is highlighted with thick lines between the *6c* light blue sites. The *2a* blue sites connect the planes. The hexagonal unit cell is marked with a thin green line. Metal ions at *2a* and *6c* sites are surrounded by four oxygen ligands each, forming axially symmetric tetrahedra around the *2a* sites (dark blue colored) and distorted tetrahedra around the *6c* sites (light blue colored). On the right side are the next metal surroundings for both crystallographic sites *2a* and *6c*.

at room temperature, has been evidenced by Co^{2+} HF-ESR spectroscopy. Measurements of the temperature dependencies of ^{27}Al NMR spectra and relaxation rates at different frequencies and magnetic fields have shown that the two-dimensional (2D) short-range order in the kagome planes of $YBaCo_3AlO_7$ develops at temperature $T_{f1} \approx 40$ K, whereas the final 3D glasslike magnetic state sets in at $T_{f2} \approx 20$ K. It appears that T_{f2} is rather similar for both compounds, as compared with the strongly different values of T_{f1}, suggesting that the kagome planes remain effectively decoupled down to low temperatures in both cases. We conclude that the major effect of the M ions that occupy both the in-plane and interplane positions is disordering of the magnetic spin lattice, which in combination with strong magnetic frustration results in a glasslike static ground state of both studied materials.

The paper is organized as follows. In Sec. II, the description of the samples and details of the experimental setups and procedures are given. Experimental results and their primary analysis are presented in Sec. III, followed by their discussion in Sec. IV. The main conclusions are summarized in Sec. V.

II. SAMPLES AND METHODS

Single crystalline samples of $YBaCo_3MO_7$ ($M =$Al, Fe) were prepared as described elsewhere [18,19]. The Co–Al–O sublattice in $YBaCo_3MO_7$ consists of kagome planes (*6c*, full lines in Fig. 1) with trigonal interplanar sites (*2a*, dashed lines in Fig. 1). This Co_3MO_7 lattice also resembles a hollow wurzite structure, while the Co_3M lattice carries common features with the pyrochlore lattice, which is often related with strong magnetic frustration. Here, Co and Al/Fe are intermixing on both sites and their relative abundances are listed in Table I. Such atomic disorder can additionally influence the magnetic frustration.

Co is solely divalent (d^7) corresponding to $S = 3/2$ and Fe is trivalent (d^5) with $S = 5/2$ [20]. As the orbital contributions

TABLE I. Co/M intermixing in $YBaCo_3MO_7$ [18,19].

M	Co/M (2a)	Co/M (6c)
Al	0.56(4)/0.44(4)	0.81(2)/0.19(2)
Fe	0.18(2)/0.82(2)	0.94(1)/0.06(1)

to the magnetic moments should be insignificant, the polar noncentrosymmetric space group ($P6_3mc$, No. 186) allows for magnetoelectric couplings, according to Dzyaloshinsky and Moriya (DM) [11,12].

NMR was measured on the ^{27}Al nuclei (spin $I = 5/2$, natural abundance 100%, quadrupole moment $Q = 0.149$ barns and the gyromagnetic ratio $\gamma_n = 11.094$ MHz T^{-1}) at constant frequencies $\nu_0 = 85.42$ and 33.28 MHz in the temperature range 6–300 K. NMR data were collected using a Tecmag pulse solid-state NMR spectrometer with a 0–9.2 T superconducting magnet from Magnex Scientific. For recording of the spectra we used a standard Hahn-echo sequence and integrated the echo intensity at each field step. The spin-lattice relaxation rate was measured by the method of stimulated echo at the maximum of line intensity.

Electron spin resonance was measured with a high-frequency/high-field setup using different components for the microwave generation and detection. In the case of $YBaCo_3AlO_7$, a backward wave oscillator (BWO) was used as a source and an InSb bolometer from QMC Instruments Ltd. as a detector. For $YBaCo_3FeO_7$, a PNA-X network analyzer from Agilent Technologies, which can be equipped with several frequency extensions was utilized. The sample was placed in the middle of an oversized waveguide inside of a homemade probe head. The latter was inserted in 16-T Oxford magnet cryostat containing a ^{4}He variable temperature insert.

Static magnetization was measured at the fields of 3 and 7 T with a superconducting quantum interference device from Quantum Design (temperature range: 1.8–400 K, 7-T magnet). In NMR and magnetization measurements, an external magnetic field was applied along the c axis, whereas ESR experiments were performed for two field directions $H \parallel c$ and $H \perp c$.

III. EXPERIMENTAL RESULTS

A. ^{27}Al NMR in $YBaCo_3AlO_7$

With nuclear magnetic resonance it is possible to probe the local magnetic fields and electron spin correlations. Almost all kind of nuclei in the crystals $YBaCo_3FeO_7$ and $YBaCo_3AlO_7$ can act as an NMR spin probe, however, NMR experiments are difficult on Y and Ba nuclei due to low sensitivity and on Co and Fe nuclei due to fast relaxation processes. For this reason, we have chosen the ^{27}Al nuclei to probe the local magnetic properties of $YBaCo_3AlO_7$.

1. NMR spectra

^{27}Al NMR spectra of a single-crystalline $YBaCo_3AlO_7$ sample were obtained by sweeping the external magnetic field applied along the c axis. ^{27}Al has a quadrupole moment, hence the relevant Hamiltonian consists of two terms resulting

from the coupling of a nucleus to its magnetic and charge environments, respectively [21]:

$$\mathcal{H} = -\gamma_n H_0 \hbar m_z + \frac{e^2 q Q}{4I(2I-1)} \frac{3\cos^2\theta - 1}{2} .$$

$$\times \left[3m_z^2 - I(I+1) + \frac{1}{2}\eta(m_-^2 - m_+^2) \right]. \quad (1)$$

Here, $\hbar$ is the reduced Planck constant, m_z and $m_\pm$ are projections of the nuclear spin I on the z-quantization axis given by the external magnetic magnetic field H_0, e is the elementary charge, q is the gradient of the electrical field, θ is the angle between H_0 and the principal axis of the electric field gradient (EFG) tensor, and η is asymmetry parameter.

Since ^{27}Al has a spin $I = 5/2$, in the presence of an electric field gradient (EFG), one can expect the occurrence of five lines in the NMR spectrum that correspond to the central transition $-\frac{1}{2} \leftrightarrow \frac{1}{2}$ and the satellites $-\frac{5}{2} \leftrightarrow -\frac{3}{2}$, $-\frac{3}{2} \leftrightarrow -\frac{1}{2}$, $\frac{1}{2} \leftrightarrow \frac{3}{2}$, and $\frac{3}{2} \leftrightarrow \frac{5}{2}$. The position of these quadrupolar satellites depends on the local charge environment. According to crystallographic refinement [18] there are two structural positions of ^{27}Al in YBaCo$_3$AlO$_7$. Half of aluminum ions (Al$_R$) occupies the regular positions ($2a$) between the kagome planes and is surrounded by the elongated oxygen tetrahedra of high symmetry. The remaining aluminum ions are defects (Al$_D$) residing in the kagome plane ($6c$). The oxygen environment of Al$_D$ is a distorted tetrahedron of a low symmetry. Because of these different charge surroundings, Al$_R$ and Al$_D$ have different quadrupolar frequencies ν_Q and a different EFG asymmetry parameter η. These two parameters were calculated using the point charge model [22] and the obtained values are listed in Table II.

As shown in Fig. 2, the ^{27}Al NMR spectrum could be reasonably well modeled by two contributions comprising five Gaussian lines each ascribed to the two distinct Al sites. For the fitting of the spectra we used the calculated quadrupolar frequencies (Table II). The width of all lines was taken equal, the linewidth and the line positions were taken as free parameters. The relative intensities of both contributions were kept equal according to the x-ray structural data. The remaining small deviations of the model spectral lines from the experimental ones are likely to originate from a distribution of the quadrupolar frequencies ν_Q resulting from the random distribution of the defects.

With decreasing temperature, the shape of the spectrum changes substantially. Due to a strong line broadening below 30 K, the quadrupolar satellites are found to overlap for Al$_R$ and the quadrupole structure is not observed anymore (Fig. 3). By approaching the temperature $T = 40$ K, the transversal relaxation time T_2 becomes one order of magnitude shorter and the decay of the echo signal starts to deviate from the

FIG. 2. Experimental ^{27}Al NMR spectrum at the fields $\mu_0 H = 3$ T (top) and 7.7 T (bottom) in the paramagnetic state at $T = 120$ K (symbols). The spectra are modeled with two contributions: the blue-colored signal (right-slanted hatching lines) is the signal from ^{27}Al at the regular position (Al$_R$), and the red-colored signal (left-slanted hatching lines) is the one from ^{27}Al in the kagome plane (Al$_D$), respectively. The black solid line represents the sum of the two contributions.

monoexponential function. This indicates different T_2 times for Al$_D$ and Al$_R$ nuclei and consequently different weights of contributions from Al$_D$ and Al$_R$ sites to the total NMR spectrum at lower T. Given this complication, the spectra in Figs. 2 and 3 were not normalized on the T_2 time.

The local magnetic fields H_{loc} cause a shift of the NMR line from the Larmor frequency $\nu_L = (\gamma_n/2\pi)H_0$, thereby the local electron spin susceptibility can be directly extracted from this shift. The so-called Knight shift K is defined as $K = (H_0 - H_{loc})/H_0$ and consists of two terms:

$$K(T) = K_{sp}(T) + K_0, \quad (2)$$

where K_0 is the temperature independent part of the shift related to the Van Vleck susceptibility and the second-order quadrupolar effects. The second-order quadrupolar shift is inversely proportional to the external magnetic field:

$$\nu_Q^{(2)}(1/2) = \frac{\nu_Q^2}{12\nu_L}[6\sin^2\theta(1 - 9\cos^2\theta)$$

$$- 4\eta\cos 2\phi\sin^2\theta(9\cos^2\theta + 1)$$

$$+ \eta^2(-16/3 + 8\cos^2\theta + 6\cos^2 2\phi\sin^4\theta)].$$

$$(3)$$

TABLE II. Quadrupolar parameters for YBaCo$_3$AlO$_7$.

	Al$_D$ ($6c$)	Al$_R$ ($2a$)
η	0.6	0
ν_Q	0.12 MHz	0.46 MHz
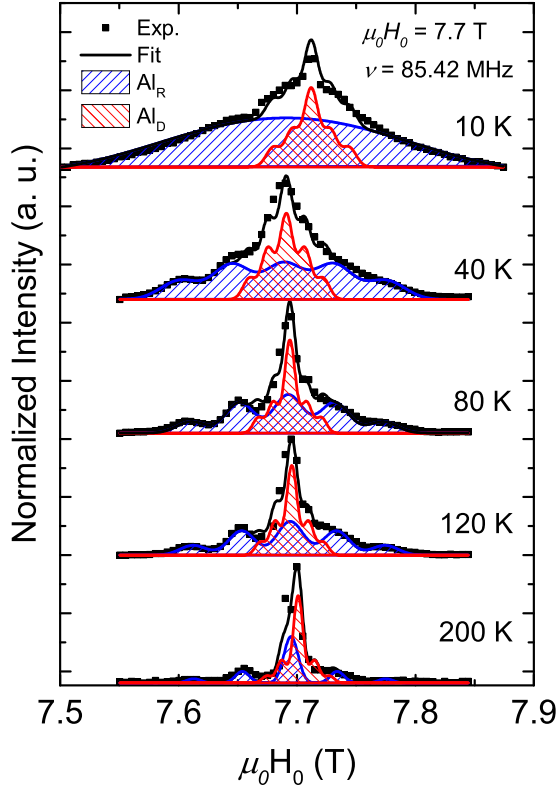
FIG. 3. Experimental ^{27}Al NMR signal at a field $\mu_0 H = 7.7$ T at different selected temperatures (symbols). The modeled contributions from ^{27}Al at the regular interplane position (Al$_R$) and at the defect position in the kagome plane (Al$_D$) are shown by the blue-colored right-slanted hatching lines and the red-colored left-slanted hatching lines, respectively. The black solid line represents the sum of the two contributions.

Here, ν_Q is the quadrupole frequency, and θ and ϕ describe the orientation of the applied magnetic field in the principal coordinate system of the EFG tensor. K_{sp} in Eq. (2) is the spin part of the shift, which is determined as

$$K_{sp}(T) = \frac{A_{hf}}{N_A \mu_B} \chi(T). \quad (4)$$

Here, A_{hf} is the hyperfine interaction constant, N_A is the Avogadro number, χ is the static spin susceptibility, and μ_B is the Bohr magneton. For further analysis of the lineshift, K_0 was subtracted from the total measured shift.

The spin part of the NMR shift K_{sp} of both contributions (Al$_D$ and Al$_R$) as a function of the bulk static susceptibility χ measured at the fields of 3 and 7 T is plotted in Fig. 4. Noting that in this plot temperature is the implicit parameter, one can conclude that K_{sp} for both Al sites follows the bulk susceptibility down to low temperatures. From a linear fit of K_{sp} versus the macroscopic susceptibility $\chi(T)$, the values of the hyperfine constants A_{hf} for both sites were determined (see Table III).

Remarkably, for Al$_D$ in the kagome plane, the $K_{sp}(\chi)$ dependence begins to deviate strongly from the high-temperature linear dependence at $T \approx 40$ K for both fields (Fig. 4, inset). Such a deviation from linearity indicates that the short-range spin correlated regime sets in at this temperature in the kagome planes and the local spin susceptibility seen by ^{27}Al$_D$ nuclei
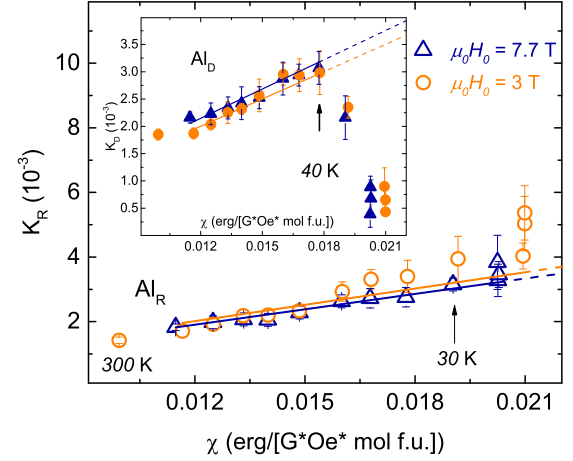
FIG. 4. ^{27}Al NMR lineshifts vs the bulk static susceptibility χ at fields of 3 and 7.7 T (circles and triangles, respectively) for the ^{27}Al nuclei at the regular Al$_R$ position (main panel, open symbols) and at the defect Al$_D$ position (inset, closed symbols). The lines are linear fits (see the text).

differs from the bulk susceptibility χ. This kind of a maximum of $K(T)$ is usually observed in the kagome-type compounds and corresponds to the temperature of about $0.2 - 0.5J$ (see, e.g., Refs. [23–26]). An estimate of the exchange interaction constant J from the susceptibility data as well as from the approximation of T_1^{-1} to $T \to \infty$ for the Al$_D$ sites [24] yields for our compound the value of about $J \sim 120$ K, implying that the maximum of K for Al$_D$ in the kagome plane occurs at $T \sim 0.3J$. For the Al$_R$ sites the line shift follows the bulk χ down to $T \approx 20$ K (Fig. 4), which is close to the freezing temperature $T_f = 16.8$ K detected in the magnetization measurement. Below 20 K, the $K_{sp}(\chi)$ dependence for this site also deviates from the linearity but in the direction opposite to the Al$_D$ line shift.

2. NMR longitudinal relaxation

The dynamics of the electron spin system is reflected in the nuclear relaxation process and can be investigated by measurements of the nuclear relaxation rates. The ^{27}Al nuclear longitudinal spin-lattice relaxation rate T_1^{-1} in YBaCo$_3$AlO$_7$ was measured at the fields $\mu_0 H = 3$ and 7.7 T corresponding to the frequencies $\nu = 33.28$ and 85.42 MHz. Above 50 K, the time evolution of the nuclear magnetization $M(t)$ can be described with a single spin-lattice relaxation time T_1 by the following function for the central transition for the nuclear spin $I = 5/2$ [27]:

$$M(t) = M_0 \left\{ 1 - f \left[\frac{50}{63} \exp\left(-\frac{15t}{T_1} \right) \right. \right.$$
$$\left. \left. + \frac{8}{45} \exp\left(-\frac{6t}{T_1} \right) + \frac{1}{35} \exp\left(-\frac{t}{T_1} \right) \right] \right\}. \quad (5)$$

TABLE III. Hyperfine coupling constants A_{hf} for YBaCo$_3$AlO$_7$.

Field (T)	Al$_R$ (kOe/μ_B)	Al$_D$ (kOe/μ_B)
3	0.92 ± 0.01	0.91 ± 0.02
7.7	0.89 ± 0.03	0.94 ± 0.03
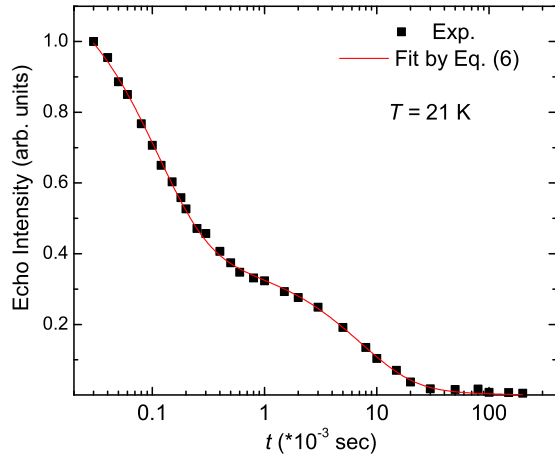
FIG. 5. Time dependence of the ^{27}Al stimulated spin echo decay at $T = 21$ K (symbols). The solid line is a fit to Eq. (6).

Here, t is the time delay between the pulses in the stimulated nuclear spin echo sequence, f is the prefactor, and M_0 is the equilibrium magnetization. However, below 50 K, the relaxation process becomes more complicated. In the decay of the stimulated spin echo two contributions with the slow and fast relaxation times can be clearly distinguished (see Fig. 5). The echo decay can be fitted as sum of two functions defined according to Eq. (5) with approximately equal weights and with two different relaxation times:

$$M(t) = M_{\mathrm{f}}(t, T_{1\mathrm{f}}) + M_{\mathrm{s}}(t, T_{1\mathrm{s}}). \qquad (6)$$

Here, $T_{1\mathrm{f}}$ and $T_{1\mathrm{s}}$ are the fast and slow relaxation times, and M_{f} and M_{s} are the fast and slow relaxing magnetization components, respectively. The temperature dependence of T_1^{-1} for both relaxation components is shown in Fig. 6. In the high-temperature regime, $T_1^{-1}(T)$ is approximately T-independent.
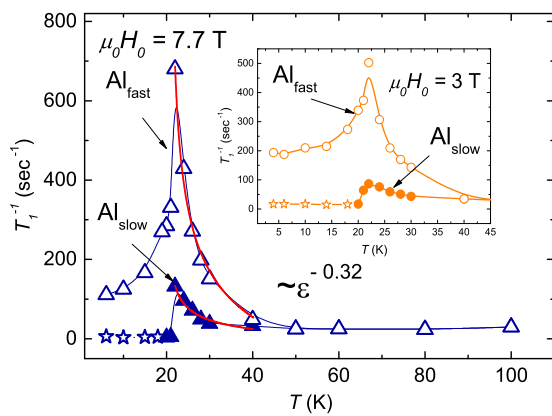
FIG. 6. Longitudinal relaxation rate T_1^{-1} of ^{27}Al nuclei as a function of temperature measured at the fields of 7.7 (main panel) and 3 T (inset). Open symbols correspond to the fast relaxing component of T_1^{-1} and filled symbols denote the slow relaxing component, respectively. Red solid lines are fits with the critical exponent (see discussion in Sec. IV). Due to technical limitations, it was difficult to measure long relaxation times. The upper limit for the corresponding slow relaxation rates is marked with stars. Lines connecting the data points are guides for the eye.
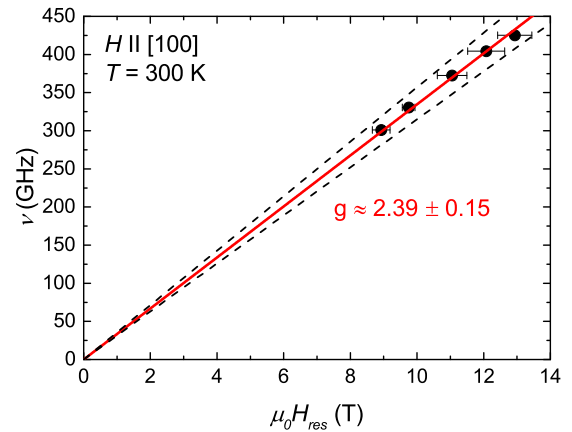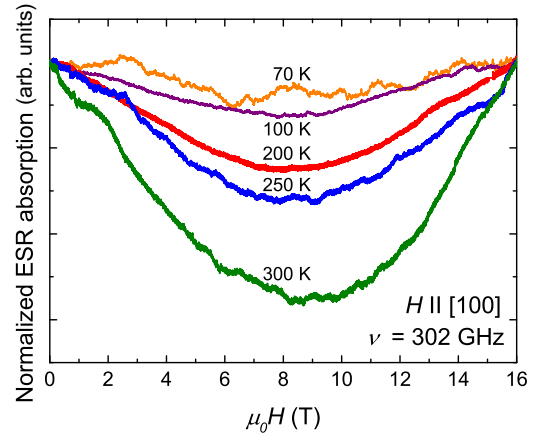
FIG. 7. HF-ESR on YBaCo$_3$AlO$_7$. Top: Spectra for several temperatures at a fixed frequency of 302 GHz. For comparison, spectra were normalized to signal intensity at zero field after subtraction of a linear background. Bottom: frequency vs resonance field dependence $\nu(H_{\mathrm{res}})$. The solid line is the fit of the data and the dashed lines show to the uncertainty range.

With further temperature decrease, the relaxation rate for both components rises and passes through a maximum around 22 K, which is the signature of the critical slowing of the antiferromagnetic spin correlations down to the NMR frequency.

B. Electron spin resonance

1. YBaCo$_3$AlO$_7$

For YBaCo$_3$AlO$_7$, an extremely broad structureless resonance signal was observed in the sub-THz frequency range as exemplary shown for several temperatures in Fig. 7(top). A linear background was subtracted from the data and, in addition, spectra were normalized to the signal intensity at zero field in order to compare spectra recorded at different temperatures. The observed resonance line extends over the whole available field range. This makes the determination of the linewidth impossible, since, obviously only the central part of the line is observed, whereas the wings of the absorption curve are out of the field range. With decreasing temperature the measured signal intensity, i.e., the height of the resonance line, decreases so that no clear signal can be observed below 100 K. Apparently, a further broadening of the line leads to reduction of signal intensity. The resonant nature of the

absorption signal was proven by room temperature measurements at several frequencies. The maximum of absorption continuously shifts to higher fields with increasing frequency. By plotting the frequency ν versus the resonance field H_{res} as in Fig. 7(bottom), the g factor can be extracted from the slope following the resonance condition for a paramagnetic state:

$$g\mu_B\mu_0 H_{res} = \nu h. \tag{7}$$

Here, μ_0 is the magnetic permeability and h is the Planck constant. Resonance fields given in Fig. 7(bottom) are obtained by averaging over resonance positions determined from four individual measurements and the respective standard deviation is used as error bar. The resulting $g = 2.39 \pm 0.15$ has a relatively big uncertainty due to large linewidth. Nevertheless, it is in agreement with Co^{2+} ions ($S = 3/2$) in a tetrahedral coordination [28], which are the only magnetic ions in this compound.

2. YBaCo₃FeO₇

For YBaCo₃FeO₇, a series of spectra for different temperatures is shown in Fig. 8. After subtracting a linear background and correcting the admixture of a dispersion signal to the data, spectra were normalized to the extremum and shifted vertically for comparison. The spectra consist of two signals, an intense line which shows a broadening for lower temperatures and a small narrow line. The second is better visible at low T, because it overlaps with the intense line at high T. The small narrow line with constant width at all temperatures is most probably due to impurities or defects. In the following, only the intense signal will be discussed.
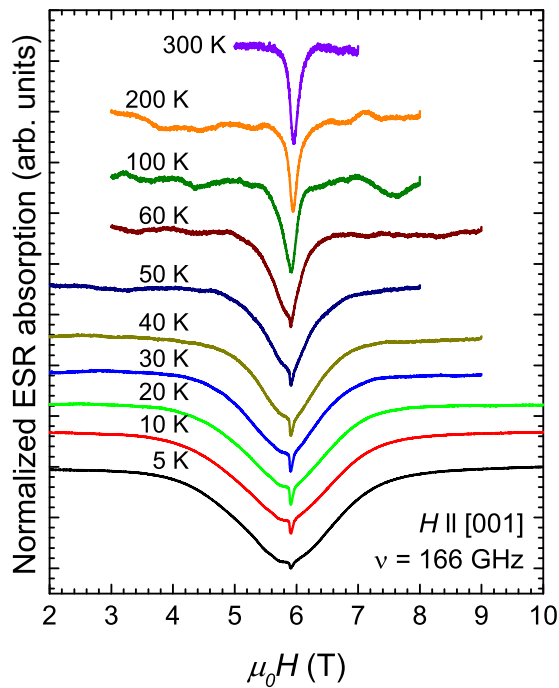
FIG. 8. HF-ESR on YBaCo₃FeO₇: spectra at $\nu = 166$ GHz for several temperatures. A linear background was subtracted from the signals and an admixture of dispersion signal to the line was corrected. Afterwards, spectra were normalized to the extremum and shifted vertically for clarity.
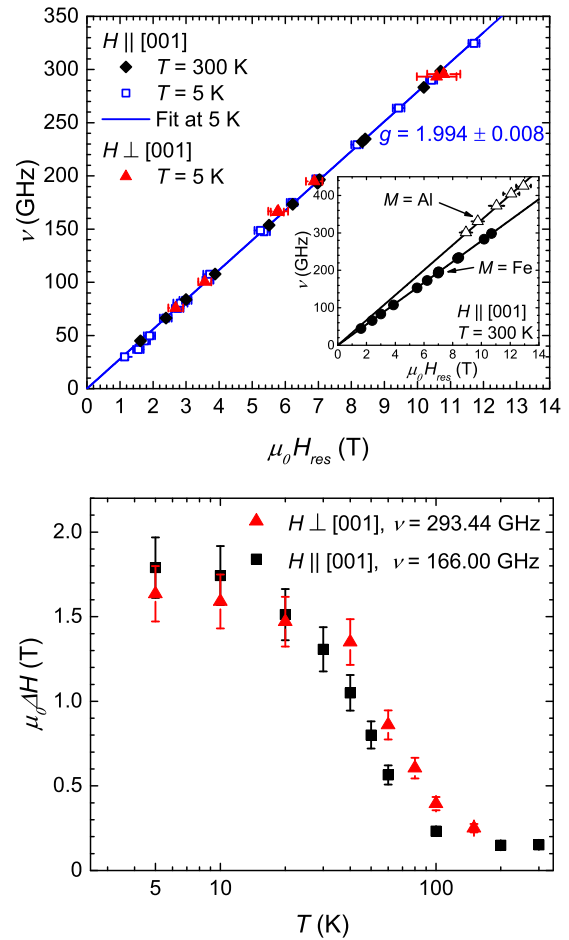
FIG. 9. HF-ESR on YBaCo₃FeO₇. (Top) Frequency resonance field dependence $\nu(H_{res})$ for different temperatures and orientations. A comparison of $\nu(H_{res})$ measured on YBaCo₃AlO₇ (open triangles) and YBaCo₃FeO₇ (filled circles) is shown in the inset. (Bottom) Temperature dependence of the linewidth ΔH for two orientations measured at different frequencies.

In addition to the temperature series, ESR measurements were performed for several frequencies at $T = 300$ and at 5 K with the external field oriented parallel to the c axis. For $T = 5$ K, the direction of H perpendicular to c ($H \parallel [1\bar{2}0]$) was also probed. In all three cases, the results show a linear dependence $\nu(H_{res})$ as depicted in the top panel of Fig. 9. Most of the points were measured for $T = 5$ K and $H \parallel c$ where the fit according to Eq. (7) yields $g = 1.994 \pm 0.008$. This value is in agreement with Fe^{3+} ions in a tetrahedral coordination since it is near to the value for the free electron, which is expected for Fe^{3+} in $3d^5$ configuration ($S = 5/2$, $L = 0$). Within the measurement uncertainty the same value was observed for $T = 300$ K and $H \parallel c$ with $g = 1.990 \pm 0.001$ and for $T = 5$ K and $H \perp c$ with $g = 1.996 \pm 0.015$. This isotropic behavior can be expected for ions with $L = 0$. Furthermore, a comparison between the spectra obtained for YBaCo₃AlO₇ and YBaCo₃FeO₇ gives additional evidence for the Fe^{3+} ions being the origin of the resonance line in YBaCo₃AlO₇. In the former compound, Co ions showed a very broad resonance line which is in contrast to the well resolved line found for the latter system. On the other hand,

considering the similar crystal structure of both compounds one might anticipate a similar resonance line from Co ions in $YBaCo_3FeO_7$, which implies that the observed line is due to the second species of magnetic ions in this compound, i.e., the Fe ions. The inset in the upper panel of Fig. 9 shows a comparison between frequency-field dependencies measured on $YBaCo_3AlO_7$ and $YBaCo_3FeO_7$. The clearly visible shift between the resonance fields for both compounds illustrates the difference in g factors found in those systems.

In the bottom panel of Fig. 9 the temperature dependence of the linewidth is plotted for the two orientations $H \parallel c$ and $H \perp c$. ΔH increases with decreasing T starting at $T_{f2} \approx$ 60 K for $H \parallel c$, which is close to the transition temperature $T_f \approx 50$ K of this compound reported in Ref. [18]. Therefore the observed signal can be attributed to the Fe ions at the interplanar sites. The broadening of the ESR signal goes along with the development of a hyperfine field as it was observed by Mößbauer spectroscopy [18].

In the HF-ESR experiments, other signals, which could be expected for the Fe at the kagome sites or the Co ions at the interplanar sites, were not detected. For the kagome sites, a short-range order with a transition temperature of $T_{f1} =$ 590 K was reported [18], which is far above the temperature range of the ESR experiment. Keeping in mind the ESR results on $YBaCo_3AlO_7$ one can suppose that the resonance signal of the kagome sites is far too broad to be observed in the available field range. There is only a minority of Co ions at the interplanar sites ($\approx 19\%$) and probably the signal intensity is too weak to be seen in the spectra.

IV. DISCUSSION

In this section, we discuss the influence of a site disorder on the magnetic properties of $YBaCo_3AlO_7$ and $YBaCo_3FeO_7$ revealed by local spin probes.

A. $YBaCo_3AlO_7$

1. ESR: effects of frustration

The observed ESR resonance line in $YBaCo_3AlO_7$ is in agreement with Co^{2+} ions in a tetrahedral coordination. The signal has an extremely large linewidth extending over the complete available field range. This suggests an extremely broad inhomogeneous distribution of internal fields fluctuating on the ESR time scale. Supposedly, the broadening increases with decreasing temperature. This behavior is very similar to other frustrated systems like $CoAl_2O_4$ where a huge broadening of the Co^{2+} ESR signal was observed for $T \lesssim |\theta_{CW}| =$ 85 K, i.e., far above the ordering temperature $T_c = 8$ K [29].

Compared to $CoAl_2O_4$, the Curie-Weiss temperature in $YBaCo_3AlO_7$, $\theta_{CW} \approx -460$ K, is much larger yielding a much higher "frustration ratio" $f = |\theta_{CW}|/T_f \approx 29$ [19]. The higher degree of magnetic frustration leads to stronger inhomogeneous spin dynamics observable at higher temperatures, which are yet smaller than θ_{CW}. This behavior is caused by the internal magnetic fields whose orientations become more and more static and random with lowering the temperature, as expected for a transition to a spin glass state. The origin is the geometrical frustration in combination with random site disorder due to the substitution of magnetic Co by nonmagnetic

Al. In ESR, the characteristic time scale is shorter than in NMR, therefore, the slowing down of the spin fluctuations can be observed at higher temperatures.

2. NMR: static properties

It is well known that an inhomogeneous broadening of an NMR line in paramagnets arises due to the distribution of local fields created by the magnetic (in our case Co^{2+}) subsystem. These fields, which are static on the NMR time scale, give a temperature dependent contribution to the total width $\Delta H = \Delta H_0 + \Delta H(T)$. Similar to the lineshift K, the linewidh $\Delta H(T)$ in the pure paramagnetic regime is proportional to the static magnetization $M = \chi H$. However, in the correlated regime, one has to take into account the extra contribution originating from the critical slowing down of Co spin fluctuations, which gives rise to additional local fields static on the NMR time scale. For the following, we subtract from the data the temperature independent part ΔH_0 that originates from the second-order quadrupolar interaction and the possible inhomogeneity of the local electric and magnetic fields due to structural distortions [30] and discuss the T-dependent contribution $\Delta H(T)$ only.

In Fig. 10, the NMR linewidths normalized to the measurement field are plotted versus the macroscopic susceptibility χ, both measured at the respective fields of 3 and 7 T, with temperature being the implicit parameter in this plot. For the $^{27}Al_D$ nuclei in the kagome plane, the linewidth starts to deviate strongly from the linear χ dependence already at 100 K followed by a peculiarity at 40 K and a slight growth of the linewidth below this temperature. For the $^{27}Al_R$ nuclei located between the kagome planes, strong deviation from linearity is observed in the low-temperature range $T \leqslant 20$ K.

In Fig. 11, we show the temperature dependence of the ^{27}Al NMR linewidth $\Delta H(T)$ for both Al positions for the measurement fields of 3 and 7.7 T. From the observed broadening of the lines, it becomes clear that the short-range correlations generating quasistatic fields that are probed by
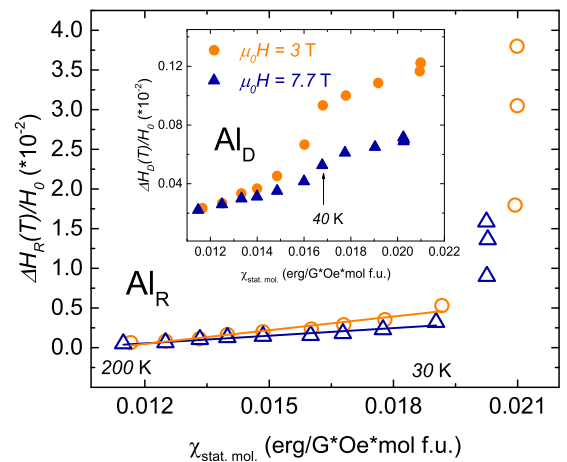
FIG. 10. ^{27}Al NMR linewidth $\Delta H(T)$ normalized to the measurement field vs the macroscopic susceptibility $\chi(T)$ at the fields of 3 (circles) and 7.7 T (triangles). Open symbols (main panel) correspond to Al_R sites in between the kagome planes, filled symbols (inset) to Al_D sites in the kagome planes, respectively. Lines are linear fits.
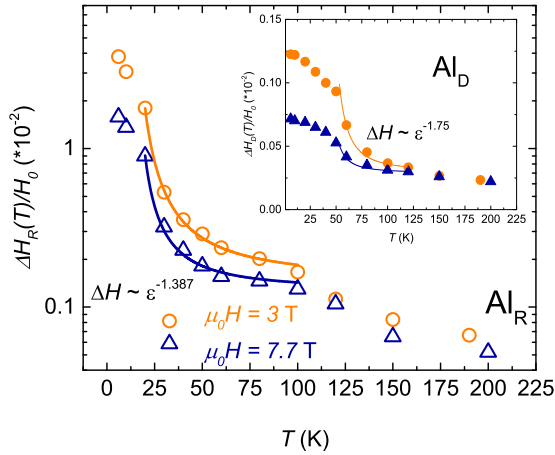
FIG. 11. Temperature dependence of ^{27}Al NMR linewidths $\Delta H(T)$ normalized to the measurement field at fields 3 (circles) and 7.7 T (triangles). Open symbols correspond to the signal from ^{27}Al$_R$ nuclei at the regular interplane positions (main panel) and closed symbols to the signal from ^{27}Al$_D$ nuclei in the kagome planes (inset). Solid lines are the respective fits $\Delta H \sim \varepsilon^\gamma$ (see the text).

the Al$_D$ sites start to develop already at $T \sim 100$ K due to a strong magnetic exchange in the kagome planes, whereas for ^{27}Al nuclei at the Al$_R$ sites in between the planes such magnetic correlations become noticeable at temperatures $T < 80$ K. For Al$_R$, the low-T upturn of the linewidth changes the slope at 20 K but still $\Delta H(T)$ continuous to increase indicating a glasslike character of the 20-K transition. The linewidth of Al$_D$ sites does not scale with magnetic field in the neighborhood of 40 K and, in contrast to Al$_R$, shows almost a plateaulike behavior below 40 K indicating the development of a static short-range order in the defect-containing kagome planes. Ultimately, the linewidth of the Al$_R$ sites reaches an approximately field independent value at lowest temperatures. Note that in Fig. 11 the linewidth $\Delta H(T)$ is normalized on the measurement field H_0 yielding smaller values of $\Delta H(T)/H_0$ at 7.7 T as compared to this ratio at 3 T.

Taking into account both, the temperature behavior of the linewidth and of the line shift (Fig. 4), one can conclude that the short-range magnetic ordering sets in the kagome planes at $T_{f1} \approx 40$ K, but no 3D long-range order occurs. Otherwise, in the 3D long-range magnetically ordered state, one can expect a shift and splitting of the NMR line without strong broadening, which is not the case here.

In an ideal 2D Heisenberg magnet, no order can occur above $T = 0$ K [31]. Indeed, in real materials, there are always weak anisotropic interplane interactions present that lead to a 3D ordering transition at finite T. The critical behavior close to this transition merely reflects the dimensionality of the magnetic subsystem in real compounds with the layered structure. As discussed above, the NMR linewidth is proportional to the local static spin susceptibility $\Delta H \sim A_{hf}\chi_{loc}$. Therefore the T dependence of ΔH in the critical regime reflects the critical temperature behavior of χ_{loc}. The latter can be described by the power law ε^γ with the critical exponent γ, where $\varepsilon = (T - T_f)/T_f$ and T_f is the critical temperature. Indeed, fitting the data points in the critical regime with the expression $\Delta H(T) \propto \varepsilon^\gamma$ yields a good agreement with experiment (Fig. 11). The

$\Delta H(T)$ dependence for the defect Al_D sites in the kagome planes can be well described with the critical exponent $\gamma = -1.75$ with $T_{f1} = 40$ K, whereas a good description of the $\Delta H(T)$ dependence for the regular Al_R sites in between the kagome planes can be achieved with $\gamma = -1.387$ and $T_{f2} = 20$ K. These values of γ are close to the critical exponents in the 2D Ising [32] and 3D Heisenberg [33] models, respectively.

The reason for the Ising-like critical behavior in the kagome planes could be related to a strongly distorted low-symmetry ligand coordination of the Co^{2+} ions in the kagome planes (Fig. 1). In this case, the low-symmetry component of the crystal field splits, due to the second-order spin-orbit coupling effects, the otherwise fourfold degenerate $S = 3/2$ spin state of Co^{2+} into two Kramers doublets $|\pm 1/2\rangle$ and $|\pm 3/2\rangle$ separated by a finite energy. This so-called zero-field splitting of the spin levels gives rise to the single ion magnetic anisotropy [28], which could result in an Ising character of the in-plane Co spins, an effect that has been observed in a number of Co-based quantum magnets (see, e.g., Refs. [34–36]). In contrast, the interplane Co^{2+} ions have a more symmetric ligand coordination rendering them Heisenberg-like. Indeed, as will be discussed below, their Heisenberg character is manifested in the dynamics. The Heisenberg-like critical behavior of $\Delta H(T)$ at the interplane ^{27}Al sites ascribed to the ordering of the interplane Co spins at $T_{f2} = 20$ K suggests that at low temperatures, they are likely to be effectively decoupled from the Ising-like in-plane Co spins, which are already frozen in a static state below $T_{f1} = 40$ K.

Additional indication of the Ising-like character of the short-range ordered state in the kagome planes comes from the analysis of the $\Delta H(T)$ dependence for the in-plane Al$_D$ sites below $T_{f1} = 40$ K, where $\Delta H(T)$ increases moderately. In this regime, the NMR linewidth should be proportional to the sublattice magnetization following the power law [37]:

$$M \sim \left(\frac{T_{f1} - T}{T_{f1}}\right)^\beta. \tag{8}$$

As can be seen in Fig. 12, $\Delta H(T)$ and $(T_{f1} - T)/T_{f1}$ indeed show a power law scaling. The obtained critical exponent $\beta = 0.11$ is significantly smaller than that for a 3D Heisenberg model ($\beta = 0.30$ [38]) and is close to the value for a 2D Ising system with $\beta = 0.125$ [32].

Even though the specific geometry of the spin lattice, the symmetry of the exchange interactions, and the degree of frustration may change to some extent the values of the critical exponents [38,39], on the qualitative level the above observations strongly support our scenario on the 2D nature of the short-range ordering in the kagome planes setting in at ~ 40 K followed by a 3D glasslike static regime below ~ 20 K.

3. NMR: dynamic properties

The 3D critical behavior is also observed in the dynamic properties. The T dependence of the relaxation rate T_1^{-1} below 60 K does not reveal any anomaly at $T_{f1} = 40$ K for both components (Fig. 6), whose absence will be discussed below. In this temperature range, it can be well fitted with the critical power law ε^p with $T_{f2} = 20$ K and $p = -0.32$ (Fig. 6), which
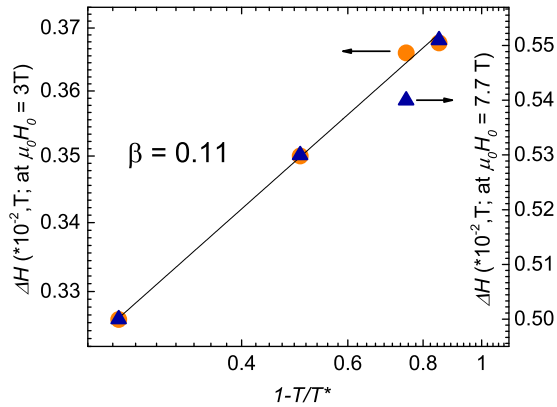
FIG. 12. Temperature dependence of the $^{27}Al_D$ NMR linewidth at the fields of 3 (left scale, filled circles) and 7.7 T (right scale, filled triangles) for the Al_D site in the kagome planes plotted as a function of the reduced temperature $(T_{f1} - T)/T_{f1}$ with $T_{f1} = 40$ K. Solid line is a fit to the data $\Delta H \sim [(T_{f1} - T)/T_{f1}]^{\beta}$ (see the text).

is close to the theoretically predicted value $p = -0.3$ for 3D Heisenberg antiferromagnets [40]. This 3D critical behavior is observed for both components, which indicates the same origin of the relaxation. In the paramagnetic regime, the Al_R and Al_D hyperfine constants are almost the same (see Table III) yielding the same relaxation rates for both aluminum sites. The difference in the local fields at different structural positions that develops in the correlated regime leads to the difference of the relaxation rates of Al_R and Al_D nuclei. The absence of the relaxation peak around $T_{f1} = 40$ K for one of the components is puzzling at first glance. However, it can be understood if to take into account that, in contrast to the linewidth, which is sensitive to the quasistatic local field parallel to the direction of the external field, the longitudinal relaxation probes only the fluctuating field perpendicular to this direction. The high planar symmetry of the metal position in the kagome plane makes the sum of the local in-plane field components produced by the local surrounding of the nonmagnetic Al_D defects in this plane almost zero in the correlated state. Thus the contributions of the in-plane cobalt spins to the nuclear spin-lattice relaxation rate of the Al_D nuclei may cancel out due to the short-range ordering. The investigations of the nuclear spin-lattice relaxation in the pure kagome compounds [24,25,41] where the origin of the relaxation is the interaction with in-plane magnetic ions, reveal a sharp decrease of the relaxation rate T_1^{-1} at low temperatures both in the spin-liquid and in the ordered states. In contrast to these compounds, in $YBaCo_3AlO_7$, there exists another, more effective at these temperatures relaxation channel for all ^{27}Al nuclei via the interaction with the interplane cobalt ions. This channel most likely dominates below 40 K where the kagome magnetic subsystem is "switched off" from the relaxation process due to the 2D short-range order. Therefore the critical behavior of the interplane cobalt subsystem is reflected in the T_1^{-1} temperature dependence of ^{27}Al nuclei at both sites.

4. Magnetic ground state

The analysis of the NMR experiments on $YBaCo_3AlO_7$ shows that there exist two independent, weakly coupled spin subsystems. Two different nuclei, $^{27}Al_D$ and $^{27}Al_R$, probe the local static and dynamic magnetism in the kagome planes and between them, respectively. One can clearly see a development of the two-dimensional critical regime in the kagome planes by approaching the temperature $T_{f1} \approx 40$ K from above, and the establishment of the 2D short-range order below this temperature. The levelling off of the T dependence of the linewidth below T_{f1} (Fig. 10) strongly supports this scenario. A decrease of the line shift below 30 K (Fig. 3, top spectrum) shows that the effective field at the Al_D nuclei decreases apparently due to the establishment of the short-range order in the kagome planes.

A 3D static state developing below $T_{f2} \approx 20$ K in $YBaCo_3AlO_7$ is reflected mostly in the NMR parameters of $^{27}Al_R$ nuclei, which, being located between the kagome planes, serve as the bulk probe of the magnetism of this compound. A continuous increase of the linewidth below T_{f2} strongly supports the conclusion in Ref. [19] of the establishment of a static spin-glass state below $T \approx 17$ K but not a 3D long-range magnetic order. The clearly observed peak in the T dependence of the relaxation rates also proves the transition to the static state. At the same time, the absence of the so-called BPP-like behavior of the relaxation peak [21] expected for classical spin glasses and the clearly observed field dependence of the relaxation rates suggest that in $YBaCo_3AlO_7$, we are not dealing with a classical spin glass but rather with a more complicated, possibly clusterlike 3D spin-glass ground state. Interestingly, a Monte Carlo study of a diluted Ising frustrated antiferromagnet [42] has shown that for a certain degree of the spin dilution, the ground state could be indeed a co-existence of the AFM short-range and spin-glass orders.

The structural disorder in $YBaCo_3AlO_7$ appears to play a manifold role: the site inversion prevents 3D long-range magnetic order as well as the spin-liquid state in the kagome planes where the nonmagnetic defects weaken the frustration and promote a short-range order in the planes. Finally, the interaction between the magnetic ions located at the defect positions between the short-range ordered kagome planes results in the cluster glasslike 3D static state of $YBaCo_3AlO_7$.

B. $YBaCo_3FeO_7$

In $YBaCo_3FeO_7$, a quasistatic state in the kagome planes establishes at a much higher temperature $T_{f1} \approx 590$ K [18]. This is obviously related to a much stronger AFM interaction strength $\theta_{CW} \approx -2000$ K as compared to $YBaCo_3AlO_7$, but also due to a partial substitution of Co^{2+} ($S = 3/2$) ions in the kagome planes by strongly magnetic Fe^{3+} ($S = 5/2$) ions. By comparing the ESR spectra obtained on $YBaCo_3AlO_7$ and $YBaCo_3FeO_7$ and considering the g factors determined by frequency-dependent measurements, it is possible to assign the observed main resonance line in the latter compound to the Fe ions. The majority of the interplane sites ($\approx 80\%$) are occupied by Fe^{3+} ions that remain effectively decoupled from the kagome planes at ambient and lower temperatures [18]. Indeed, their essentially paramagnetic behavior is observed in the HF-ESR experiment. Therefore, in analogy to the nuclear spins of Al_R in $YBaCo_3AlO_7$, the Fe electron spins can sensitively probe the establishment of the interplane 3D correlations.

1. ESR of interplanar Fe sites

The ESR signal of the Fe ions at the interplanar sites shows a linear dependence $\nu(H_{res})$ with $g = 1.994$ at $T = 300$ K (Fig. 9, top), a behavior that is expected for paramagnetic spins. A similar behavior at a much lower temperature $T = 5$ K (Fig. 9, top) suggests that the spins do not order long-range magnetically even at low temperatures. Otherwise, an opening of the magnetic anisotropy gap for spin excitations associated with the long-range magnetic order would cause a nonlinearity and gapped behavior of the $\nu(H_{res})$ dependence [43]. The broadening of the ESR signal (Fig. 9, bottom) goes along with the development of a hyperfine field as it was observed by Mößbauer spectroscopy [18]. On the other hand, the temperature dependence of the resonance fields does not show an indication for the establishment of a state with long-range order. Thus the broadening of the line with decreasing temperature can be understood as a slowing down of spin fluctuations at the interplanar sites. The continuous freezing of the spin dynamics gives rise to randomly oriented quasistatic moments. This leads to an inhomogeneous broadening of the ESR line without shifting the resonance field. This picture is supported by the isotropic g factor, which was measured parallel and perpendicular to the kagome planes. The broadening is observed at slightly higher temperatures than $T_f \approx 50$ K for two possible reasons. First, the characteristic time scale of ESR is shorter than in Mößbauer spectroscopy making it possible to observe the slowing down earlier. Second, in the ESR experiment, an additional external field is applied, which can further affect the spin dynamics. Indeed, for the second orientation $H \perp c$, which was measured at a higher field, the broadening starts already at $T \approx 100$ K (Fig. 9, bottom).

2. Interlayer spin correlations

In Ref. [18], neutron scattering experiments on $YBaCo_3FeO_7$ are presented and modeled using Monte Carlo simulations based on a classical Heisenberg Hamiltonian which takes into account nearest-neighbor interactions only. These calculations revealed the development of strong quasi-one-dimensional spin correlations between the interlayer sites along the c direction below 50 K. As a result, in this temperature regime, a ferromagnetic alignment of spins at the interlayer sites is realized along the c axis, while neighboring interlayer spins in the $a-b$ plane are rotated by $120°$ with respect to each other [18,44]. However, in the ESR investigations presented above, an isotropic behavior of the resonance position is observed. At 5 K, resonance fields are not shifted when changing the orientation of the external field from being aligned parallel to c to lying perpendicular to c. In addition, there is no shift in the resonance position for $H \parallel c$ between 5 and 300 K. On the other hand, such shifts would be expected due to ferromagnetic alignment of spins along c as this leads to a change in the strength and the orientation of the local magnetic fields. Thus our ESR results suggest that the model describing the magnetism in $YBaCo_3FeO_7$, so far, requires further elaboration in order to cover all experimental findings.

V. CONCLUSIONS

In summary, we have undertaken a detailed experimental study with ESR and NMR spectroscopic techniques of the electron spin dynamics in single crystals of the spin frustrated magnets $YBaCo_3MO_7$ (M=Al, Fe) with the layered kagome-type crystal structure. Previous studies of the title compounds have revealed strong and frustrated antiferromagnetic interactions between the spins of the transition metal ions in the kagome planes. No long-range magnetic order was observed in both compounds. Instead, they were found to exhibit a glasslike freezing of the spin lattice at low temperature, which was attributed to the structural disorder and strong magnetic frustration.

In our work, we have obtained new interesting insights into the peculiar magnetism of $YBaCo_3MO_7$ (M=Al, Fe). The use of the local ESR (Fe^{3+}, Co^{2+}) and NMR ($^{27}Al_R$ and $^{27}Al_D$) spin probes located at different positions of the spin lattice has enabled us to disentangle the spin dynamics and magnetic correlations due to the intraplane and interplane magnetic couplings. We have identified two distinct, weakly interacting subsystems which could not be resolved by bulk methods. In the case of $YBaCo_3AlO_7$, we could clearly observe the development of the 2D correlations in the kagome planes exhibiting an Ising-like critical behavior over an extended temperature range that finally results in a short-range ordered state in the kagome planes at $T_{f1} \approx 40$ K. Furthermore, we could distinguish the development of the magnetic correlations between the interplanar Co sites, which appear to be more Heisenberg-like and yield a static state below $T_{f2} \approx 20$ K. Our data confirm that this state is not long-ranged ordered. Considering previous data in Ref. [19], this state is rather glasslike.

In the case of $YBaCo_3FeO_7$, we observe that the Fe spins located in between the kagome planes are effectively decoupled from the planes and remain dynamic down to $T_{f2} \approx 60$ K. Below this temperature, the resonance response of this spin subsystem does not show signatures typical for a long-range order but indicate a continuous glasslike freezing of the spin dynamics. Remarkably, our results evidence isotropic spin correlations between the interplanar Fe sites, which calls for a revision of the previously conjectured scenario of the one-dimensional spin correlations along the c axis.

It follows from our results that despite the different types of partial substitution in $YBaCo_3MO_7$ of Co by nonmagnetic Al and magnetic Fe, respectively, and substantially different temperature scales T_{f1} for the establishment of the static magnetic state in the kagome planes, the final 3D magnetic ground state sets in at rather similar temperatures T_{f2} of ≈ 20 and ≈ 60 K, respectively. NMR and ESR local spin probes reveal a gradual establishment of the 3D spin correlations, which eventually evolve into a frozen glasslike spin state in both materials. It appears that the major effect of the partial substitution of the Co ions by M ions (M=Al, Fe) in both the in-plane and interplane positions is the occurrence of disorder in the spin network of the coupled kagome planes. The resulting randomness of the exchange interactions between magnetic ions and reduction of the magnetic frustration gives rise to a quasistatic short-range ordered state in the kagome planes at elevated temperatures that finally develops into a 3D glass state at a low temperature.

[1] P. Babkevich, P. Freeman, M. Enderle, D. Prabhakaran, and A. Boothroyd, Nat. Commun. **7**, 11632 (2016).

[2] J. Fujioka, Y. Yamasaki, H. Nakao, R. Kumai, Y. Murakami, M. Nakamura, M. Kawasaki, and Y. Tokura, Phys. Rev. Lett. **111**, 027206 (2013).

[3] K. Takada, H. Sakurai, E. Takayama-Muromachi, F. Izumi, R. Dilanian, and T. Sasaki, Nature (London) **422**, 53 (2003).

[4] J. V. Badding, Nat. Mater. **2**, 208 (2003).

[5] A. C. Masset, C. Michel, A. Maignan, M. Hervieu, O. Toulemonde, F. Studer, B. Raveau, and J. Hejtmanek, Phys. Rev. B **62**, 166 (2000).

[6] J.-M. Chen, Y.-Y. Chin, M. Valldor, Z. Hu, J.-M. Lee, S.-C. Haw, N. Hiraoka, H. Ishii, C.-W. Pao, K.-D. Tsuei, J.-F. Lee, H.-J. Lin, L.-Y. Jang, A. Tanaka, C.-T. Chen, and L. H. Tjeng, J. Am. Chem. Soc. **136**, 1514 (2014).

[7] L. L. Balents, Nature (London) **464**, 199 (2010).

[8] O. A. Starykh, Rep. Prog. Phys. **78**, 052502 (2015).

[9] C. Rüegg, Nat. Phys. **6**, 837 (2010).

[10] A. Ramirez, *Handbook of Magnetic Materials* (Elsevier Science, Amsterdam, 2001).

[11] I. Dyzaloshinsky, J. Phys. Chem. Solids **4**, 241 (1958).

[12] T. Moriya, Phys. Rev. **120**, 91 (1960).

[13] A. Huq, J. Mitchell, H. Zheng, L. Chapon, P. Radaelli, K. Knight, and P. Stephens, J. Solid State Chem. **179**, 1136 (2006).

[14] V. Caignaer, V. Pralong, A. Maignan, and B. Raveau, Solid State Comm. **149**, 453 (2009).

[15] J. D. Reim, E. Rosen, W. Schweika, M. Meven, N. Leo, D. Meier, M. Fiebig, M. Schmidt, C. Y. Kuo, T. W. Pi, Z. Hu, and M. Valldor, J. Appl. Cryst. **47**, 2038 (2014).

[16] M. Valldor, J. Phys: Condens. Matter **16**, 9209 (2004).

[17] W. Schweika, M. Valldor, and P. Lemmens, Phys. Rev. Lett. **98**, 067201 (2007).

[18] M. Valldor, R. P. Hermann, J. Wuttke, M. Zamponi, and W. Schweika, Phys. Rev. B **84**, 224426 (2011).

[19] M. Valldor, N. Hollmann, J. Hemberger, and J. A. Mydosh, Phys. Rev. B **78**, 024408 (2008).

[20] N. Hollmann, Z. Hu, M. Valldor, A. Maignan, A. Tanaka, H. H. Hsieh, H.-J. Lin, C. T. Chen, and L. H. Tjeng, Phys. Rev. B **80**, 085111 (2009).

[21] C. Slichter, *Principles of Magnetic Resonance* (Springer, New York, 1989).

[22] J. D. Jackson, *Classical Electrodynamics* (John Wiley & Sons Inc., Hoboken, NJ, 1998).

[23] P. Mendels, A. Keren, L. Limot, M. Mekata, G. Collin, and M. Horvatić, Phys. Rev. Lett. **85**, 3496 (2000).

[24] Z. Hiroi, M. Hanawa, N. Kobayashi, M. Nohara, H. Takagi, Y. Kato, and M. Takigawa, J. Phys. Soc. Jpn. **70**, 3377 (2001).

[25] A. Olariu, P. Mendels, F. Bert, F. Duc, J. C. Trombe, M. A. de Vries, and A. Harrison, Phys. Rev. Lett. **100**, 087202 (2008).

[26] J. A. Quilliam, F. Bert, R. H. Colman, D. Boldrin, A. S. Wills, and P. Mendels, Phys. Rev. B **84**, 180401 (2011).

[27] A. Narath, Phys. Rev. **162**, 320 (1967).

[28] A. Abragam and B. Bleaney, *Electron Paramagnetic Resonance of Transition Ions* (Clarendon Press, Oxford, 1970).

[29] M. Iakovleva, E. Vavilova, H.-J. Grafe, S. Zimmermann, A. Alfonsov, H. Luetkens, H.-H. Klauss, A. Maljuk, S. Wurmehl, B. Büchner, and V. Kataev, Phys. Rev. B **91**, 144419 (2015).

[30] P. Jeglič and J.Dolinšek, Phys. Rev. B **71**, 014204 (2005).

[31] N. D. Mermin and H. Wagner, Phys. Rev. Lett. **17**, 1133 (1966).

[32] J. Binney, N. Dowrick, A. Fisher, and M. Newman, *The Theory of Critical Phenomena: An Introduction to the Renormalization Group* (Oxford University Press, Oxford, 1992).

[33] J. C. le Guillou and J. Zinn-Justin, Phys. Rev. Lett. **39**, 95 (1977).

[34] R. Coldea, D. A. Tennant, E. M. Wheeler, E. Wawrzynska, D. Prabhakaran, M. Telling, K. Habicht, P. Smeibidl, and K. Kiefer, Science **327**, 177 (2010).

[35] O. Breunig, M. Garst, E. Sela, B. Buldmann, P. Becker, L. Bohatý, R. Müller, and T. Lorenz, Phys. Rev. Lett. **111**, 187202 (2013).

[36] S. K. Niesen, G. Kolland, M. Seher, O. Breunig, M. Valldor, M. Braden, B. Grenier, and T. Lorenz, Phys. Rev. B **87**, 224413 (2013).

[37] M. Nishiyama, S. Maegawa, T. Inami, and Y. Oka, Phys. Rev. B **67**, 224435 (2003).

[38] H. Kawamura, J. Phys. Soc. Jpn. **61**, 1299 (1992).

[39] M. F. Collins and O. A. Petrenko, Can. J. Phys. **75**, 605 (1997).

[40] H. Benner and J. Boucher, in *Magnetic Properties of Layered Transition Metal Compounds*, edited by L. D. Jongh (Kluwer, Dordrecht, Boston, London, 1990).

[41] N. E. Sherman, T. Imai, and R. R. P. Singh, Phys. Rev. B **94**, 140415 (2016).

[42] C. Wendel, C. L. Henley, and A. Zippelius, Phys. Rev. B **53**, 6543 (1996).

[43] E. A. Turov, in *Physical Properties of Magnetically Ordered Crystals*, edited by A. Tybulewicz and S. Chomet (Academic Press, New York, 1965).

[44] D. D. Khalyavin, P. Manuel, J. F. Mitchell, and L. C. Chapon, Phys. Rev. B **82**, 094401 (2010).